ISSN: 2321-2152

IJMECE

International Journal of modern electronics and communication engineering

E-Mail
editor.ijmece@gmail.com
editor@ijmece.com

www.ijmece.com

ISSN 2321-2152
www.ijmece.com
Vol 13, Issue 2, 2025

A Novel Approach To MIMO Control For Interleaved buck converters in EV DC Fast Charging Applications

[1] S. Padma Sharon, [2]Shaik Abusaleha,[3]Bolikonda Vilas, [4]Boodula Manasa, [5]Mood Siva Naik, [6]Neeluru Haritha,
[1]Assistant Professor, Department of EEE, Ananthalakshmi Institute Of Technology And Sciences, Itikalapalli, Near Sk University,Ananthapur.
[2,3,4,5,6] Student, Department of EEE, Ananthalakshmi Institute Of Technology And Sciences, Itikalapalli, Near Sk University,Ananthapur.

Abstract—

In this short, we provide a novel method of controlling off-board DC fast chargers for electric vehicles (EVs). To improve the performance of interleaved dc buck converters over standard PI/PID controls, the suggested feedback matrix architecture prevents repeated tuning of controllers in several and linked loops. rapid adjustment of both load fluctuations and imbalances among the legs, as well as reference current monotonic monitoring from any beginning state of charge with an arbitrarily rapid settling time, are new aspects of the described technique. When compared to traditional PI/PID controls, the suggested discrete-time MIMO technique for interleaved buck converters significantly improves performance, according to the numerical findings. Proving the proposal's viability and efficacy are findings from experiments using both full-scale hardware-in-the-loop (HIL) and smaller prototypes. Electric vehicle (EV), interleaved converter, hardware-in-the-loop (HIL), and multiple input multiple output (MIMO) control are index terms.

INTRODUCTION A SIGNIFICANT

the development of small, lightweight switch power supplies with improved efficiency, rapid dynamic response, and minimal steady-state error in the presence of parametric component uncertainties and load changes has been a prolific topic of study in recent years. By interleaving the currents in each phase, the interleaved multiphase converter can increase the switching frequency, decrease the size and weight of the converter, improve the total current ripple, and reduce switching and conduction losses [1, 2]. The cheap price and well standardized parallel modules are two other benefits. Current sharing control, on the other hand, is crucial to the interleaved method and is heavily impacted by switch on resistance or inductance mismatches [3]. This is because to the inherent margins of error in building materials, which include The manufacturer has a hard time controlling temperature fluctuations when the converter legs are operating, and there is a color version of at least one figure in this article available. Losses and heat dissipation become imbalanced when current sharing is not equal. So, depending on the change of numerous detected signals, a distinct control action is required for each leg to operate this converter. Since current sharing enhances system performance by reducing transient response and thermal issues, it is essential when combining several phases [4,5]. Multiple and linked PI/PID controllers are the most often used control mechanisms in the literature (see references 6, 7, and 8). The average duty cycle is often calculated by a main controller using the converter's transfer function, which is produced by averaging in state space. The imbalance between the remaining "slave" legs and one "master" leg is balanced out by a second set of secondary controls. Not being able to withstand big disturbances and uncertainty is the biggest problem with the widely used PID-based control technique [9]. This issue may be resolved with nonlinear sliding mode control. Nevertheless, data on the state vector and more precise parameter values are necessary. In [10], PI controllers are used to modify the duty ratio that is produced by the sliding mode control for each phase. Fuzzy controllers, on the other hand, don't need any background information on the converter, which is its primary benefit. Nevertheless, owing to their complicated and heuristic decision-making processes—including fuzzification, rule base storage, an inference mechanism, and defuzzification—fuzzy logic controllers need a significant amount of processing power [11]. Using the methodology first presented in [12] and expanded upon in [13], we provide a novel multiple input multiple output (MIMO) control technique in this short to circumvent these restrictions. This approach, which is called global monotonicity, is based on the idea of designing a feedback matrix that guarantees a monotonic response from any initial condition with

ISSN 2321-2152
www.ijmece.com
Vol 13, Issue 2, 2025

an arbitrarily fast settling time. It does this by imposing a closed-loop eigenstructure where each component of the tracking error is driven only by a single real-valued closed loop mode. This design eliminates overshoot and undershoot. This is the only method that can make the system's output monotonic in every output component, independent of the system's starting state, as shown in [13]. The present need for innovative control techniques in the automobile industry to reduce greenhouse gas (GHG) emissions and enhance urban air quality is met by the proposed MIMO control [14]. Electric vehicles (EVs) that use renewable energy to power their batteries may reduce emissions by as much as 30 percent compared to cars driven by thermal engines [15]. Because there is a strong relationship between battery price, longevity, charging time, and the features of the used battery charger, battery technology is crucial to the spread of EVs [16]. There are primarily three power levels of battery chargers. Specifically, the rapid chargers are part of stage three. These chargers provide high dc power straight to the battery; they are off-board and often found in public charging stations. Reducing costs and making the charging time comparable with traditional petroleum refill are the main difficulties for these chargers [17], [18], [19].

To achieve these goals, many converter topologies have been suggested in the literature, such as the multilevel neutral point clamped (NPC) converter [21] and the Vienna rectifier [20]. The buck converter is a common component in dc-dc charger stages due to its well-known design techniques and straightforward construction. The following are the three main categories into which Lithium-ion (Li-ion) battery charging strategies fall: Using historical experimental data, empirical model-oriented charging controllers may predict battery states and compute electrical components. Fuzzy, linear quadratic, or model predictive control may enhance the battery charge in certain instances. 2) Algorithms for controlling the battery's temperature distribution that are based on models of electrochemistry batteries with the goal of reducing charging times. 3) Approaches that do not need models, such as pulse charging, multistage CCCV, constant-current (CC), and constant-voltage (CCCV). References [22], [23], and [24] cover the key pros and cons of various control algorithms. For electric vehicles, the CC-CV is now the standard charging procedure [25]. Experimentation has confirmed the suggested MIMO control's performance, and simulations have compared it to alternative approaches. These are the key aspects of this converter management that allow for dc rapid charging of electric vehicles. 1) Multiple-input multiple-output (MIMO) control systems are designed to prevent adjusting multiple-PI/PID controllers in multiple-connected loops. 2) In contrast to the controlled system matrix, which has real and stable eigenvalues, the interleaved buck converter's system matrix contains two complex conjugate eigenvalues. 3) While the areal-time method manages the state variables' steady-state values, the feedback matrix dictates how the system behaves dynamically. 4) Assuming any starting point, it is guaranteed that the tracking error will drop monotonically. This guarantees that the response will neither overshoot or undershoot. 5) A configuration parameter in the process may be adjusted to force the reference current step response settling time.

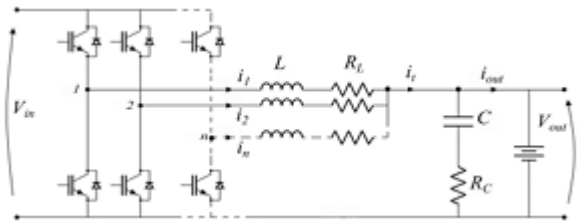

Fig. 1. N-leg interleaved buck converter for EV fast charging applications.

When the system parameters change, the closed-loop system adjusts the current/load set point and any imbalances in current between the legs. Here is how the brief is structured. Part II details the power converter's discrete-time state-space concept. Chapters III and IV detail the tracking control issue and the suggested n-leg interleaved buck converter control, correspondingly. Numerical, real-time, and experimental findings achieved utilizing a Li-ion rechargeable battery pack are reported in Section VI, while Section V gives a comparison with alternative approaches. Conclusions taken from this investigation are presented in the concluding section.

INTERLEAVED BUCK CONVERTER CIRCUIT AND DISCRETE-TIME STATE-SPACE MODEL

ISSN 2321-2152
www.ijmece.com
Vol 13, Issue 2, 2025

The typical off-board electric vehicle charger consists of an ac-dc converter for power grid interface and a dc-dc converter for charging the battery. This short examines a dc-dc converter, specifically an n-leg interleaved buck converter, as seen in Figure 1. At this point, Vin stands for the input voltage (dc-link voltage), while iout and Vout are the symbols for the current and voltage, respectively, that are output. The power stage of each leg consists of an inductor with L inductance and RL coupling resistance, two insulated gate bipolar transistors (IGBTs) switches with on-state resistance RSw, and so on. All j-leg equivalent series resistances (ESRs) are defined as

$$R_{sj} = R_{Swj} + R_{Lj}, \quad j = 1, 2, \ldots, n. \tag{1}$$

Toggling the power switches is done using pulse-width modulation (PWM) signals that are 360 degrees/n apart and have duty cycles d1(k), d2(k),..., dn(k) that range from 0 to 1. Each phase shares the filter capacitance C and the parasitic series resistance RC. We may ignore the RC effects and approximatively get VC for the output voltage and iout for the total current if the ESR of the capacitor is small enough.

$$i_t(k) = \sum_{j=1}^{n} i_j(k) \approx i_{out}. \tag{2}$$

$$\Sigma : \begin{cases} x(k+1) = A\,x(k) + B\,u(k), & x(0) = x_0 \\ y(k) = C\,x(k) \end{cases} \tag{3}$$

where the vectors

$$x(k) = \begin{bmatrix} i_1(k) \\ \vdots \\ i_n(k) \\ V_C(k) \end{bmatrix}, \quad u(k) = \begin{bmatrix} d_1(k) \\ \vdots \\ d_n(k) \end{bmatrix}, \quad y(k) = \begin{bmatrix} i_1(k) \\ \vdots \\ i_n(k) \end{bmatrix} \tag{4}$$

symbolize, in that order, the them-dimensional state (with m= n+1), the then-dimensional control input (which contains duty-cycle signals as components), and the then-dimensional output. The system matrix, B, is a matrix that belongs to the real matrix family Rm×n, while C is a matrix that belongs to the real matrix family Rn×m. With the zero-order-hold discretization approach and sampling time Ts, these matrices may be produced via the continuous-time state-space model of the interleaved buck converter (see [8]).

GLOBALMONOTONICTRACKING

The term "global monotonic tracking" describes the challenge of creating a state-feedback control rule for a multiple-input multiple-output (MIMO) linear time-invariant system that allows the output y to follow the preferencer with zero steady-state error and monotonicity in all components, regardless of the beginning circumstances. It is both non-overshooting and non-undershooting if y is monotone and asymptotically follows the constant reference r. Assuming the following (for example, refer to [26]) about the discrete-time system: it is right invertible, stable, and does not have any invariant zeros at 1; we then continue as follows: our initial step is to design a seafeedback gain matrix F such that A+BF stable as x approaches infinity. For the given variable r, find two stable state vectors xss and uss that fulfill the linear equation.

$$x_{ss} = A\,x_{ss} + B\,u_{ss}, \qquad r = C\,x_{ss}. \tag{5}$$

$$\Sigma_{aut} : \begin{cases} \xi(k+1) = (A + B\,F)\,\xi(k), & \xi(0) = x_0 - x_{ss} \\ y(k) = C\,\xi(k) + r. \end{cases} \tag{7}$$

Assuming stabilizability, the uncontrolled eigenvalues of the A+BF system are stable, and the other eigenvalues may be arbitrarily assigned to be stable and fast enough to increase the response speed, thereby controlling the dynamics of the closed-loop system. As t approaches infinity, x converges to xss, ξ converges to zero, and y converges to r since A+BF is asymptotically stable. Ensuring that the tracking error ϵ(k)=y(k)−r(k) converges monotonically to 0 in all components from all beginning circumstances is crucial if we are to achieve our aim of selecting F in a fashion that guarantees global monotonicity from any initial state. In turn, this means that the tracking mistake must have a structural

$$\epsilon(t) = \left[\beta_1\,\lambda_1^k, \ldots, \beta_n\,\lambda_n^k\right]^T \tag{8}$$

The values λ1,..., λn are stable since they are closed-loop eigenvalues. Put otherwise, if we can get a tracking error ϵ(t) with one power per component and |λk|

ISSN 2321-2152
www.ijmece.com
Vol 13, Issue 2, 2025

$$\begin{bmatrix} A-\lambda_j I & B \\ C & 0 \end{bmatrix}\begin{bmatrix} v_j \\ w_j \end{bmatrix} = \begin{bmatrix} 0 \\ \beta_j e_j \end{bmatrix} \quad (9)$$

whereβj≠0andej isthe jthvectorofthestandardbasisof Rn: (9)alwayshasasolutioninviewof theright- system's invertibility. By selecting F such that Fvj=wj, we get (A+BF)vj=λjvj and Cvj=βjej.. The answer is therefore, for each ξ0∈ span{vj}

$$\epsilon(k) = e_j \gamma_j \lambda_j^k \quad (10)$$

ηj is dependent on ξ0. By extending this approach to all components of the tracking error, we get a set of solutions v1 w1, v2 w2,..., vn wn of (9), considering λ1,...,λn ∈(−1,1). For any integer i from 1 to n, we may select F such that Fvi = wi if v1,..., vn are linearly independent. So, by superimposing, we discover ξ0 for every v1, v2,..., vn.

$$\epsilon(k) = \begin{bmatrix} \gamma_1 \lambda_1^k \\ 0 \\ \vdots \\ 0 \end{bmatrix} + \begin{bmatrix} 0 \\ \gamma_2 \lambda_2^k \\ \vdots \\ 0 \end{bmatrix} + \begin{bmatrix} 0 \\ 0 \\ \vdots \\ \gamma_n \lambda_n^k \end{bmatrix} = \begin{bmatrix} \gamma_1 \lambda_1^k \\ \gamma_2 \lambda_2^k \\ \vdots \\ \gamma_n \lambda_n^k \end{bmatrix}. \quad (11)$$

We need to make the remaining m−n closed-loop modes invisible at ϵ for this response to be attainable from any beginning state. By taking use of the system's supremal stabilizability output-nulling subspace V⋆ g, this job may be completed. The image of [V1 V2 •• Vd] that meets may be obtained as this subspace.

$$\begin{bmatrix} A-\mu_j I & B \\ C & 0 \end{bmatrix}\begin{bmatrix} V_j \\ W_j \end{bmatrix} = 0 \quad (12)$$

Given another matrix [W1 W2 •• Wd] that is partitioned in a certain way, where {μ1,...,μt} are the minimum-phase invariant ant zeros of and {μt+1,...,μd} are stable and arbitrary (for example, let's suppose they are real and distinct for simplicity). Each initial state ξ0 may be expressed as the sum of ξv and ξr, where ξv is a vector in V⋆ g and ξr is a vector in span{v1,v2,...,vn}, if the dimension of V⋆ g+span{v1,v2,...,vn} is equal to m. If the difference between dimV and g is less than or equal to m-n, and we can get a set of columns {vn+1,...,vm} from the data in [V1 V2 •• Vd] that are linearly independent of {v1,...,vn}, we may use wn+1,...,wm as the columns in Wg that correspond to vn+1,...,vm, and build the feedback control ω(k) = Fξ(k) where Fi is such that Assuming that (11) is still applicable, the response associated with ξv is zero, and the one associated with ξr is provided by [w1 ••• wn wn+1 ••• wm]. The tracking error may thus be expressed as in (8) for every ξ0. {λ1,...,λn} is the union of the closed-loop eigenvalues produced with F and the set of μj associated with the columns {vn+1,...,vm} selected from [V1 V2 •• Vd].

INTERLEAVEDBUCKCONVERTER MIMOCONTROL

The CCCV method is one of the several accessible and commonly used ways for charging Li-ion batteries. By choosing a charging profile consisting of two primary modes, this method lessens the detrimental impacts on the performance of the converter and the battery caused by voltage and current spikes. There is a preponderance of constant current control modes in EV fast charging stations because they allow for rapid charging of large SOC values. Then, with continuous voltage management, the charging current may progressively decrease until it reaches the ultimate value of the output current [22]. To meet the parameters (zero steady-state tracking error under the reference signal i∗ t, asymptotic stability, and nonovershooting/nonundershooting dynamics), the proposed technique relies on implementing two separate control algorithms, with a focus on the constant current control mode. The steady-state values of the status and control vectors xss and uss, as functions of the reference current i■ t, the open circuit battery voltage VOC, the battery droop coefficient Rand, and the leg resistances, are computed using the first method during the battery charging process (1). It is readily shown that

ISSN 2321-2152
www.ijmece.com
Vol 13, Issue 2, 2025

$$x_{ss} = \begin{bmatrix} \frac{i_l^*}{n} \\ \frac{i_l^*}{n} \\ \frac{i_l^*}{n} \\ i_l^* R + V_{OC} \end{bmatrix}, \quad u_{ss} = \begin{bmatrix} \frac{V_{OC} + i_l^* \left(R + \frac{R_{s1}}{n}\right)}{V_{in}} \\ \frac{V_{OC} + i_l^* \left(R + \frac{R_{s2}}{n}\right)}{V_{in}} \\ \frac{V_{OC} + i_l^* \left(R + \frac{R_{s3}}{n}\right)}{V_{in}} \end{bmatrix}$$

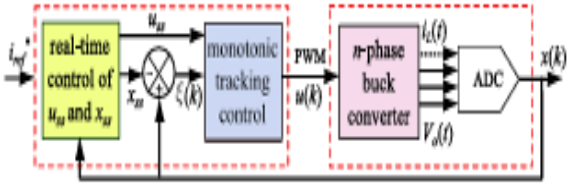

Fig.2. Blockdiagramcomprisingconverterandcontrol scheme.

TABLEI
PARAMETERVALUESOFTHEINTERLEAVEDBUCKC ONVERTERCIRCUI

Symbol	Parameter	a) Simulation/HIL	b) Experiment
n	Number of legs	3	3
L	Filter Inductance	344 μH	680 μH
C	Filter Capacitance	16.0 μF	100 μF
R_L	Inductor ESR	300 mΩ	173 mΩ
R_{Sw}	Leg ESR	20 mΩ	70 $m\Omega$
V_{in}	DC-Input voltage	618 V	24.0 V
i_l^*	Output ref. current	125 A	2.50 A
f_{sw}	Switching freq.	20 kHz	20 kHz
f_s	Sampling freq.	60 kHz	60 kHz
A/D	ADC resolution	12 bit	12 bit

COMPARISON WITH CONVENTION AL PIAN DPIDF

In contrast to the PI/PIDF average controls reported in[6] and[8] with reference to Table Ia), a full-scale scenario with a 3.84 resistive load was used to assess the performance of the proposed technique under parameter changes and model uncertainties. A principal controller in these current-balance controllers uses the converter averaging model to calculate the average duty cycle. In order to make up for the leg imbalances, secondary PI controllers determine the duty ratio. Specifically, PIDF controllers—discrete controllers with a PID structure and a filter—are presented in [8] as an indirect digital design technique. Based on an analytical design technique called "inversion formulae," which explicitly express the controller parameters in terms of the design specifications given by the phase/gain margins and the corresponding crossover frequencies, this method is based on a pole zero cancellation technique. For more information on this, see [29]. In order to ensure an equitable comparison, the PI controller PI=Kp+Ki(Ts/(z−1)) has been constructed to get a non-monotonic response according to the control technique outlined in [6]. The phase margin is 71 degrees and the crossover frequency is 3000 rad/s when the values of Kp are 0.15 e−3 and Ki are 18.16, specifically. For the PIDF tuning, these are the same design criteria mentioned in [29]. The following discrete-time system matrices describe the state-space model of the buck converter:

$$A = \begin{bmatrix} 0.9620 & -0.0226 & -0.0226 & -0.0410 \\ -0.0226 & 0.9620 & -0.0226 & -0.0410 \\ -0.0226 & -0.0226 & 0.9620 & -0.0410 \\ 0.8823 & 0.8823 & 0.8823 & 0.7002 \end{bmatrix}$$

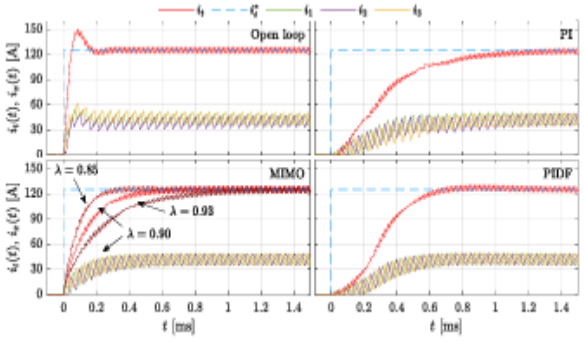

Fig. 3. Step responses usingduty cycles

ISSN 2321-2152
www.ijmece.com
Vol 13, Issue 2, 2025

d1,2,3 =79.8%inopen loop, the suggested MIMO global monotonic tracking approach, and PI/PIDF average control schemes (refer to [6], [8]).

$$B = \begin{bmatrix} 29.511 & -0.2326 & -0.2326 \\ -0.2326 & 29.511 & -0.2326 \\ -0.2326 & -0.2326 & 29.511 \\ 14.040 & 14.040 & 14.040 \end{bmatrix}, \quad C = \begin{bmatrix} 1 & 0 \\ 0 & 1 \\ 0 & 0 \end{bmatrix}$$

starting from scratch. It is therefore possible to stabilise this system as it is entirely accessible. There is a minimal phase invariant zero at 0.7597, and a straightforward computation reveals that it is right invertible. The state variables and control signals' steady-state values are dynamically computed using the formula (13). Uss = [0.798 0.798 0.798]⊦ and xss = [41.66 41.66 41.66 480.0]⊦ are the corresponding values. For a worldwide monotonic response, the gain matrix F was designed using the global monotonic tracking approach. Specifically, the initial value of the closed-loop system has been chosen to be equal to the invariant zero of the system to be managed, Λ1=0.7597, since m♯n=1. In order to maintain a balanced current sharing in the converter, the values of the other three eigenvalues, λ2, λ3, and λ4, have been selected in the stability unit circle and are equal to each other. In order to get the appropriate settling time in the step response, the control may be adjusted to a value of λ that is between 0 and 1. When this value is set to λ=0.90, the associated feedback gain matrix becomes
With a constant duty cycle of 79.8 percent in an open loop and the three approaches discussed, Fig. 3 shows the step responses of the inductor currents and the total current. The condition of zero tracking error is met in all circumstances. A quicker response—58% compared to the PI controller and 41% to the PIDF controller—is, unsurprisingly, the benefit of the suggested method. By adjusting the value of λ as a degree of freedom, the settling time may be changed; for example, setting λ=0.9 results in a settling time of 1.2 ms. Figure 3 shows various settling times for the values λ ∈{0.85,0.90,0.93}. Restrictions on the

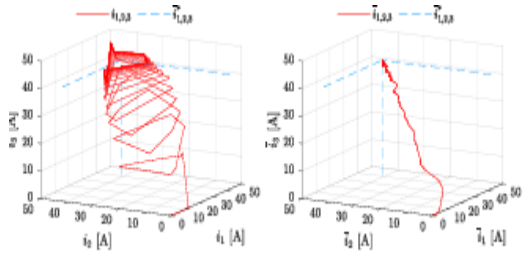

Fig.4. State-spacetrajectoriesoftheinstantaneous(left)andaveraged(right) interleavedcurrentsusingglobalmonotonictracking control.

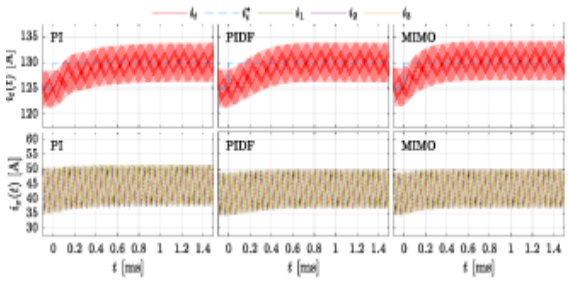

Fig.5. Setpoint i∗ t variationfrom125to130AusingPI,PIDF,andglobal monotonictrackingmethods. TABLEII LI-IONBATTERYPARAMETERS

Symbol	Parameter	a) Simulation/HIL	b) Experiment
V_n	Nominal voltage	477 V	4 × 3.70 V
C_r	Rated capacity	50 Ah	2.5 Ah
T_r	Response time	30 s	-
V_c	Cut-in voltage	555 V	16.8 V
V_d	Cut-out voltage	-	4 × 4.20 V
R_i	Internal resistance	95 mΩ	-
V_e	Exponential voltage	515 V	-
C_e	Exponential capacity	2.46 Ah	-

The location of the duty cycles to be within the interval [0,1] in (4) determines the speed of the step response. In Figure 4(right), we can see the state-space trajectories of the averaged injector currents at steady-state convergence. As shown in Figure 4 (left), the size of the closed route is connected to the current's peak-to-peak ripple. The instantaneous currents then stabilize along this path. Figure 5 displays the results for a step-type modification of i■

ISSN 2321-2152
www.ijmece.com
Vol 13, Issue 2, 2025

t (t) from the nominal value 125-130A. All the situations that are being examined have zero tracking error because of the controls. In comparison to the 0.6 and 0.5 seconds of the PI and PIDF controllers, the approach described in this short produces the quickest response of 0.3 seconds.

NUMERICALANDEXPERIMENTAL VALIDATION

Numerical, real-time hardware-in-the-loop (HIL), and experimental testing using the converter parameters and battery models from Tables I and II have all been conducted on the proposed MIMO control structure. Tables Ia) and IIa) include full-scale scenarios used for comparison with other approaches and real-time HIL validation, whereas Tables Ib) and IIb) provide data for the scaled-down experimental prototype. Quantitative Findings Derived from Shepherd's Li-Ion Battery Model The MATLAB-Simulink (MathWorks) batteryblock has been used to get numerical simulation results, where

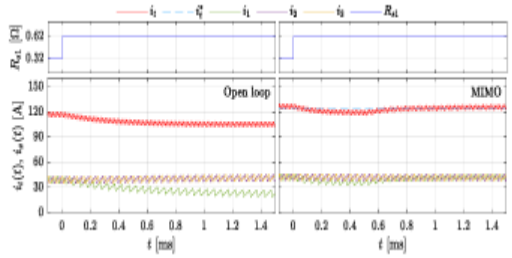

Fig. 7. Responses under step variation of Rs1 from 0.32 to 0.62 of the open-loop system versus the proposed MIMO control.

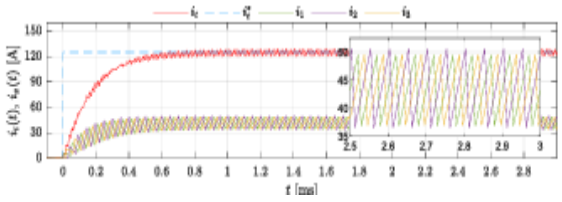

Fig. 8. Proposed method step response with an L2 10% inductor reduction.

The values for the battery model are taken from Table II and are based on the Shepherd's model [30]. As mentioned in Section V, the control is put into action by using the feedback gain matrix F. Figure 6 displays the outcomes of a step-variation of i∏ t from 0 to 125 A, with λ = 0.85 for a SOC of 20%. Low state-of-charge (SOC) battery packs linked to rapid charging infrastructure are anticipated to have a charging rate of 2.5 C, which is the reference current that has been selected. In 0.5 milliseconds, the currents consistently follow the reference value i■ t /3 with no steady-state error. We have also run simulations with SOC 20% and 70% to see whether this outcome holds true regardless of the starting point. The tracking mistake disappears monotonically in every instance. Figure 7 displays the control of the output current and inductor currents as a function of Rs1. A change from 0.32 to 0.62 in the resistance of the first leg series occurred at t = 0 ms. In 0.7 ms, the legs have balanced out, proving that, unlike in the open loop case, the control accounts for changes in resistance among the legs. Last but not least, simulations have been run to test how well the suggested control technique holds up when faced with inductor value uncertainties. This is important since inductors are among the components whose nominal values are most susceptible to such ambiguity. Figure 8 displays the total and inductor currents as a function of the reference step variations at L2 = 0.9 L. The inductor current waves from peak to peak are not symmetrical, but the overall current mean value matches the reference signal with a steady state inaccuracy of around 0.8 ms.

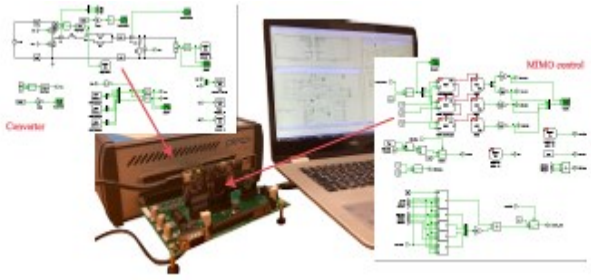

Fig. 9. Real-time HIL experimental setup.

B. Validation in Real-Time using HIL The experimental setup in Fig. 9 was used to gather HIL data, which verify the real-time practicality. Table Ia: The full-scale converter plant on a separate control card, while the TMS320F28379D digital signal processor (DSP) from Texas Instruments ran the controller, which was simulated in real-time within

ISSN 2321-2152
www.ijmece.com
Vol 13, Issue 2, 2025

the RT-Box 1 (Plexim). We have used the external mode feature to gather results after deploying both RT-Box 1 and DSPexecution codes in a PLECS (Plexim) environment. With real execution timings, synchronized PWM generation, and sensing/conversion delays, this test may be used to confirm that a commercial DSP is feasible. We have replicated the full-scale converter using a discretization step of 2.38 µs and the identical battery parameters from Section VI-A (refer to Table IIa) with a starting state of charge of 50%. This model captures all the key features of the genuine full-scale prototype. In order to put the control into action, we reuse the feedback gain matrix F from Section V. Our simulation findings were used to validate the step response, current balance, and resilience under parameter uncertainty. In Figure 10, we can see the same Rs1 step as in Section VI-A; however, in contrast to Figure 7, the actual DSP returns the HIL current balance in around 0.6 ms. Under inductor uncertainty (L2 = 0.9L), the HIL step response is seen in Fig. 11. Besides a little altered peak-to-peak range for the current ripple, there is no average drift or mismatch in the current. A monotonic tracking response in about 0.6 ms is guaranteed by the proposed MIMO control. C. Trial and Error Testing on a Miniature Model In order to test how well the suggested MIMO control works with the dc charger, we used the configuration in Figure 12. One example is the buck converter that uses three phases interleaved.

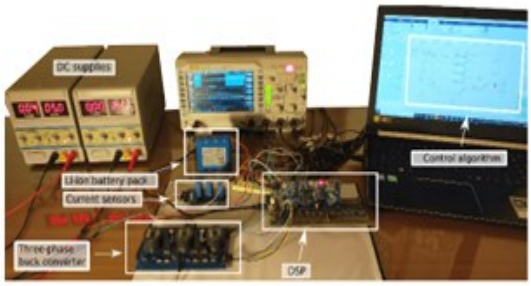

Fig.12. Scaled-downexperimental setup.

defined by the variables presented in Tables Ib) and IIb). To provide galvanic isolation between the converter power board and the DSP side, three LES6-NP(LEM)Halleffectcurrentsensors have been used to monitor the inductors' currents. With the exception of a 2.5V offset, the current sensors' output signals are directly proportional to the measured current. In order to communicate with the DSP control card's 3.3V 12-bit analog-to-digital converter (ADC), a specialized conditioning circuit has been developed. The HIL findings are generated by the same digital signal processor (DSP) that drives the converter's bipolar junction transistors (BJTs). See Table IIb for details on the four 18650 cells that make up the Li-ion rechargeable pack battery. Each cell has a nominal voltage of 3.7V. The high-performance batterypacks made by top-tier electric vehicle manufacturers (like Tesla Inc.) rely heavily on this kind of battery cell. CodeComposerStudio (Texas Instruments) IDE was used to deliver the executable code to the DSP target after the suggested MIMO control was built in MAT LAB/Simulink. Using a sample rate ranging from 5 to 250 MSa/s, experimental findings were collected using the theoscilloscope DS1054Z (Rigol). With no starting conditions, the experimental converter model is defined by the matrices

$$A = \begin{bmatrix} 0.992 & -0.002 & -0.002 & -0.024 \\ -0.002 & 0.992 & -0.002 & -0.024 \\ -0.002 & -0.002 & 0.992 & -0.024 \\ 0.163 & 0.163 & 0.163 & 0.966 \end{bmatrix}$$

$$B = 10^{-4} \begin{bmatrix} 5861 & -3.969 & -3.969 \\ -3.969 & 5861 & -3.969 \\ -3.969 & -3.969 & 5861 \\ 484.0 & 484.0 & 484.0 \end{bmatrix}, \quad C = \begin{bmatrix} 1 & 0 & 0 & 0 \\ 0 & 1 & 0 & 0 \\ 0 & 0 & 1 & 0 \end{bmatrix}$$

The predicted state/input variables xss = [0.83330.83330.833314.80]⊦ and uss = [0.6250.6250.625]⊦ are matched by the experimental currents of the inductor and the output voltage at steady-state. A globally monotonic response was achieved by applying the suggested approach to the experimental converter. Specifically, the first eigenvalue of in

ISSN 2321-2152
www.ijmece.com
Vol 13, Issue 2, 2025

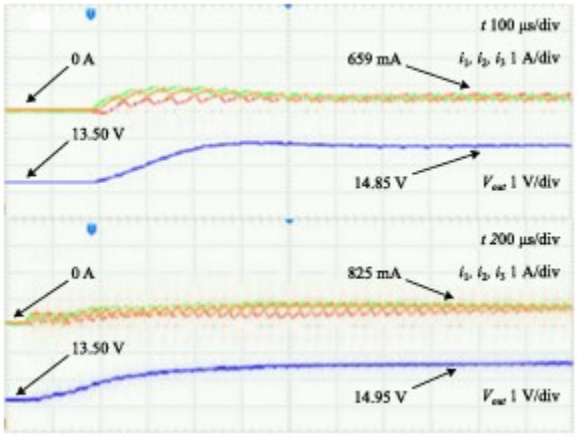

Fig. 13. StepresponsesusingLi-ionbatterypackfromVOC=13.5Vin open-loop (top) withdutycycle equal to62.5%and theproposedMIMO globalmonotonictrackingmethodswithi∗ t =2.5A(bottom).

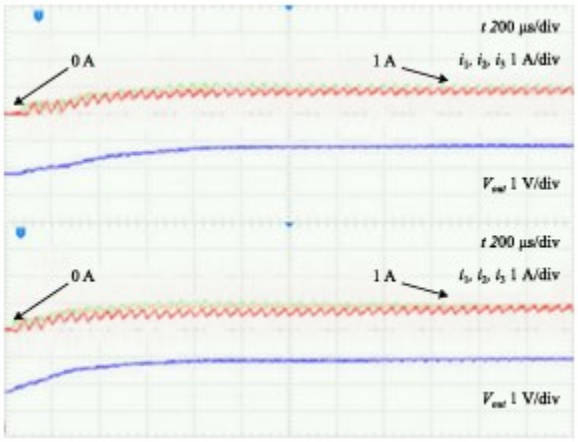

Fig.14. StepresponsesusingLi-ionbatterypackwithi∗ t =3A,λ=0.985 (top)andλ=0.980(bottom).

For the closed-loop system to maintain a balanced current sharing among the converter legs, it has been chosen to be equal to the invariant zero of the system to be regulated. The values of the other three eigenvalues have been picked in the stability unit circle and are equal to each other. A feedback gain matrix is obtained by setting these values to λ∈{0.972,0.985,0.985,0.985}.

$$F = 10^{-4}\begin{bmatrix} -118 & 34.3 & 34.3 & 411 \\ 34.3 & -118 & 34.3 & 411 \\ 34.3 & 34.3 & -118 & 411 \end{bmatrix}.$$

Using a duty-cycled=62.5% open-loop technique, the test findings showed steady reactions from VOC equivalent to 13.5V. Fig. 13 shows the top and bottom frames, respectively, of the proposed MIMO global monotonic tracking technique with λ=0.985 and i∏ t = 2.5A(1Cchargingrate). Take note that the inductor currents' steady-state values are monotonically monitored, but with open-loop control, there is a current overshoot of twice the needed magnitude and the steady-state value is around 20% lower than intended. The BJT voltage drop, unexplained losses, and other various nonideal factors are to blame for this open-loop discrepancy.

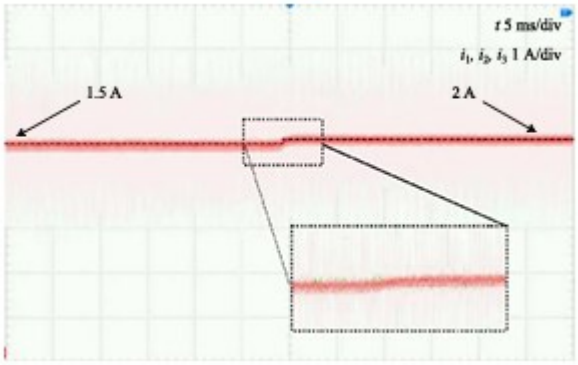

Fig. 15. Inductor currents under +33% i∗ t step variation from 1.5 to 2 A.

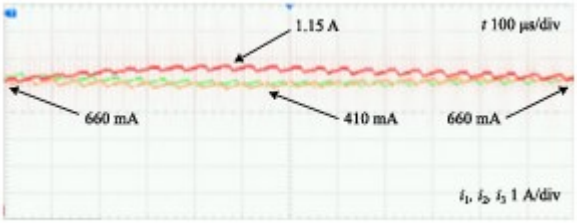

Fig. 16. Proposed control during a 1.5 Rs1 variation with i∗ t = 2 A. on.

With the MIMO control technique, the target value is achieved in around 1.1 ms after compensating for

actual system phenomena. Figure 14 shows the results of testing the global monotonic tracking technique with λ = 0.985 and λ = 0.980, respectively, under step fluctuations of i∏ t from 0 to 3 A. A lower value of λ results in a quicker reaction, much as what is seen in Figure 3. For this specific scenario, a settling time of 1.1 ms is produced by λ = 0.985, while a value of 1 ms is produced by λ = 0.98. Once again, there is no overshoot and the steady state is attained. The currents that are interleaved are shown in Figure 15, which shows the results of varying the set point i■ t from 1.5 to 2 A. Large EV charging facilities are likely to experience the +33% current increase that is seen when power is reallocated after the EV disconnection [31]. In less than 1 millisecond, the suggested MIMO control achieves steady-state behavior free of oscillations. At last, we have additionally tried the suggested technique with a variation of Rs1, which is a 1.5 reduction of the starting value. In under 1.2 milliseconds, as seen in Figure 16, the legs' unbalanced current sharing was corrected. As the system changes, i1 increases by almost 74%, peaking at 1.15 A, while i2 and i3 fall by nearly the same amount, falling to 410 mA. All things considered, a full-scale numerical validation of our MIMO control's efficacy has been carried out. Using a real-time HIL configuration, the same situation has been examined. The suggested control architecture successfully achieves the required performance, as verified by a scaled-down prototype.

CONCLUSION

This brief covered a novel method of multiple-input multiple-output control for dc-dc interleaved buck converters used in electric vehicle DC rapid charging operations. While enhancing the converter's dynamical behavior in comparison to conventional PI/PID regulators, the suggested control method eliminates the need to tune controllers in several linked loops. Our simulations have shown that, regardless of the starting point of the battery charge, and regardless of reference current step and load fluctuations, the tracking error disappears monotonically. Additionally, it is shown that the suggested management may even out disparities between the legs caused by variations in parasite resistances or components' aging. Experiments with both full-scale HIL and smaller-scale configurations have validated the theoretical and computational analyses using the suggested control framework. A sensor-less technique using estimators is being considered for future advancements with the goal of accomplishing a current balancing action without the usage of a specialized transducer [32].

REFERENCES

[1]. R. G. Retegui, M. Benedetti, M. Funes, P. Antoszczuk, and D. Carrica, “Current control for high-dynamic high-power multiphase buck con verters,” IEEE Trans. Power Electron., vol. 27, no. 2, pp. 614–618, Feb. 2012.

[2]. O. Garcia, P. Zumel, A. de Castro, and J. A. Cobos, “Automotive DC–DC bidirectional converter made with many interleaved buck stages,” IEEE Trans. Power Electron., vol. 21, no. 3, pp. 578–586, May 2006.

[3]. X. Zhou, P. Xu, and F. C. Lee, “A novel current-sharing control technique for low-voltage high-current voltage regulator module appli cations,” IEEE Trans. Power Electron., vol. 15, no. 6, pp. 1153–1162, Nov. 2000.

[4]. D. Schumacher, P. Magne, M. Preindl, B. Bilgin, and A. Emadi, “Closed loop control of a six phase interleaved bidirectional DC–DC boost converter for an EV/HEV application,” in Proc. IEEE Transp. Electrific. Conf. Expo (ITEC), Jun. 2016, pp. 1–7.

[5]. L. Ni, D. J. Patterson, and J. L. Hudgins, “High power current sen sorless bidirectional 16-phase interleaved DC–DC converter for hybrid vehicle application,” IEEE Trans. Power Electron., vol. 27, no. 3, pp. 1141–1151, Mar. 2012.

[6]. G. Balen, A. R. Reis, H. Pinheiro, and L. Schuch, “Modeling and control of interleaved buck converter for electric vehicle fast charg ers,” in Proc. Brazilian Power Electron. Conf. (COBEP), Nov. 2017, pp. 1–6.

[7]. H.-C. Chen, C.-Y. Lu, and U. S. Rout, “Decoupled master-slave current balancing control for three-phase interleaved boost converters,” IEEE Trans. Power Electron., vol. 33, no. 5, pp. 3683–3687, May 2018.

[8]. S. Cuoghi, R. Mandrioli, L. Ntogramatzidis, and G. Gabriele, “Multileg interleaved buck converter for EV charging: Discrete-time model and direct control design,” Energies, vol. 13, no. 2, p. 466, Jan. 2020.

[9]. K. E. L. Marcillo et al., "Interval robust controller to minimize oscil lations effects caused by constant power load in a DC multi-converter buck-buck system," IEEE Access, vol. 7, pp. 26324–26342, 2019.
[10]. M. H. Mahmud, Y. Zhao, and Y. Zhang, "A sliding mode duty ratio control with current balancing algorithm for interleaved buck converters," in Proc. IEEE Appl. Power Electron. Conf. Exposit. (APEC), Mar. 2018, pp. 2281–2287.
[11]. M. Leso, J. Zilkova, and P. Girovsky, "Development of a simple fuzzy logic controller for DC–DC converter," in Proc. IEEE 18th Int. Power Electron. Motion Control Conf. (PEMC), Aug. 2018, pp. 86–93.
[12]. R. Schmid and L. Ntogramatzidis, "A unified method for the design of nonovershooting linear multivariable state-feedback tracking con trollers," Automatica, vol. 46, no. 2, pp. 312–321, Feb. 2010.
[13]. L. Ntogramatzidis, J.-F. Trégouët, R. Schmid, and A. Ferrante, "Globally monotonic tracking control of multivariable systems," IEEE Trans. Autom. Control, vol. 61, no. 9, pp. 2559–2564, Sep. 2016.
[14]. J. M. Blanes, R. Gutiérrez, A. Garrigós, J. L. Lizán, and J. M. Cuadrado, "Electric vehicle battery life extension using ultracapacitors and an FPGA controlled interleaved buck-boost converter," IEEE Trans. Power Electron., vol. 28, no. 12, pp. 5940–5948, Dec. 2013.
[15]. Electric Vehicles From Life Cycle and Circular Economy Perspectives, Eur. Environ. Agency, Copenhagen, Denmark, 2018.
[16]. M. Y. Metwly, M. S. Abdel-Majeed, A. S. Abdel-Khalik, R. A. Hamdy, M. S. Hamad, and S. Ahmed, "A review of integrated on-board EV battery chargers: Advanced topologies, recent developments and opti mal selection of FSCW slot/pole combination," IEEE Access, vol. 8, pp. 85216–85242, 2020.
[17]. M. Yilmaz and P. T. Krein, "Review of battery charger topologies, charging power levels, and infrastructure for plug-in electric and hybrid vehicles," IEEE Trans. Power Electron., vol. 28, no. 5, pp. 2151–2169, May 2013.
[18]. W.-S. Lee, J.-H. Kim, J.-Y. Lee, and I.-O. Lee, "Design of an iso lated DC/DC topology with high efficiency of over 97% for EV fast chargers," IEEE Trans. Veh. Technol., vol. 68, no. 12, pp. 11725–11737, Dec. 2019.
[19]. K. Drobnic et al., "An output ripple-free fast charger for elec tric vehicles based on grid-tied modular three-phase interleaved con verters," IEEE Trans. Ind. Appl., vol. 55, no. 6, pp. 6102–6114, Nov. 2019.
[20]. J. Channegowda, V. K. Pathipati, and S. S. Williamson, "Com prehensive review and comparison of DC fast charging converter topologies: Improving electric vehicle plug-to-wheels efficiency," in Proc. IEEE 24